JBC Papers in Press. Published on November 19, 2019 as Manuscript RA119.011695
The latest version is at http://www.jbc.org/cgi/doi/10.1074/jbc.RA119.011695

Mitochondrial oxidants, but not respiration, are sensitive to glucose in adipocytes

James R. Krycer[1,2], Sarah D. Elkington[1,2], Alexis Diaz-Vegas[1,2], Kristen C. Cooke[1,2], James G. Burchfield[1,2], Kelsey H. Fisher-Wellman[5], Gregory J. Cooney[2,3], Daniel J. Fazakerley[1,2,4,#,*], David E. James[1,2,3,*]

From the [1]School of Life and Environmental Sciences, The University of Sydney, Sydney, NSW 2006, Australia; [2]Charles Perkins Centre, The University of Sydney, Sydney, NSW 2006, Australia; [3]Sydney Medical School, The University of Sydney, Sydney, NSW 2006, Australia; [4]Metabolic Research Laboratories, Wellcome Trust-Medical Research Council Institute of Metabolic Science, University of Cambridge, Cambridge, CB2 0QQ, UK; [5]East Carolina Diabetes and Obesity Institute, Brody School of Medicine, East Carolina University, Greenville, NC 27834, USA

Running title: *Mitochondria sense supply and demand in adipocytes*

[#] Current address: Metabolic Research Laboratories, Wellcome Trust-Medical Research Council Institute of Metabolic Science, University of Cambridge, Cambridge, CB2 0QQ, UK

*To whom correspondence should be addressed:
David E. James: Charles Perkins Centre, The University of Sydney, Sydney, NSW, 2006, Australia; david.james@sydney.edu.au; Tel. (612) 8627 1621
Daniel J. Fazakerley: Metabolic Research Laboratories, University of Cambridge, Cambridge, CB2 0QQ, UK; djf72@medschl.cam.ac.uk; Tel. (441) 223 748 178

Keywords: Adipocyte, glucose, insulin, mitochondria, respiration, oxidative stress, insulin resistance

ABSTRACT

Insulin action in adipose tissue is crucial for whole-body glucose homeostasis, with insulin resistance being a major risk factor for metabolic diseases such as type 2 diabetes. Recent studies have proposed mitochondrial oxidants as a unifying driver of adipose insulin resistance, serving as a signal of nutrient excess. However, neither the substrates for nor sites of oxidant production are known. Since insulin stimulates glucose utilisation, we hypothesised that glucose oxidation would fuel respiration, in turn generating mitochondrial oxidants. This would impair insulin action, limiting further glucose uptake in a negative feedback loop of 'glucose-dependent' insulin resistance. Using primary rat adipocytes and cultured 3T3-L1 adipocytes, we observed that insulin increased respiration, but notably this occurred independently of glucose supply. In contrast, glucose was required for insulin to increase mitochondrial oxidants. Despite rising to similar levels as when treated with other agents that cause insulin resistance, glucose-dependent mitochondrial oxidants failed to cause insulin resistance. Subsequent studies revealed a temporal relationship whereby mitochondrial oxidants needed to increase before the insulin stimulus to induce insulin resistance. Together, these data reveal that a) adipocyte respiration is principally fuelled from non-glucose sources, b) there is a disconnect between respiration and oxidative stress, whereby mitochondrial oxidant levels do not rise with increased respiration unless glucose is present, and c) mitochondrial oxidative stress must precede the insulin stimulus to cause insulin resistance, explaining why short-term insulin-dependent glucose utilisation does not promote insulin resistance. These data provide additional clues to mechanistically link nutrient excess to adipose insulin resistance.

Adipose tissue is a key nutrient sensor in mammals (1). Being highly sensitive to insulin, adipocytes respond to nutrient replete conditions by increasing energy intake and storage as lipid. Conversely, under nutrient excess, adipocytes become insulin resistant, leading to increased lipid utilisation and reduced glucose intake. Indeed, impaired glucose uptake into adipose tissue is one of the earliest defects observed in whole-body insulin resistance, in both rodents and humans (e.g., (2-

4)). Furthermore, knocking out GLUT4 specifically in the adipose tissue results in whole-body insulin resistance in mice (5). Thus, adipocyte insulin sensitivity appears critical for whole-body glucose homeostasis.

Insulin resistance in adipose tissue can be caused by numerous insults such as chronic hyperinsulinaemia, inflammation, and corticosteroids. Each of these have been examined in isolation through *in vivo* (mouse) and *in vitro* (adipocyte) models (e.g., (6,7)), revealing that they all produce mitochondrial oxidants (mitoROS) as a potential unifying cause of insulin resistance (reviewed in (8)). Although impaired mitochondrial function has been observed in insulin resistance (9,10), we have recently shown that acute treatment with mitochondrial-targeted paraquat (mPQ) increased mitoROS and caused insulin resistance, without impacting mitochondrial respiration (11). This supports the notion that mitoROS alone, without defects in mitochondrial respiration, is sufficient to cause insulin resistance. This raised the possibility that under physiological circumstances, insulin resistance may arise without defects in mitochondrial respiration, but rather as a result of oxidation of specific substrates (e.g., glucose, fatty acids) generating mitoROS. This suggests that mitoROS might represent a mechanistic sensor for nutrient excess (12), particularly in the adipocyte.

Since insulin potently promotes glucose uptake into adipocytes, we considered the role of glucose utilisation in adipose insulin resistance. We have previously observed that insulin stimulates glucose oxidation (13), glucose-fuelled TCA cycle flux (Quek *et al*., *under review*), and respiration (14) in adipocytes. Thus, we hypothesised that insulin stimulates respiration and subsequent mitoROS production in a glucose-dependent manner, with insulin resistance stemming from glucose oversupply. Such 'glucose-dependent' insulin resistance would limit further glucose uptake as a form of negative feedback.

Using respirometry and metabolic labelling, we found that glucose was not required for insulin-stimulated respiration in cultured and primary adipocytes. In contrast, the insulin-stimulated increase in mitoROS was glucose-dependent. This presents a physiological disconnect between mitochondrial respiration and oxidative stress – although both increase in response to insulin, they have distinct substrate requirements. Furthermore, insulin-stimulated oxidant generation did not cause insulin resistance, at least acutely, despite mitoROS rising to levels observed with other agents that induce insulin resistance (11). This was because mitoROS needed to increase prior to the insulin stimulus, demonstrating that the timing of oxidative stress is crucial in the development of insulin resistance. These observations provide additional clues to mechanistically link nutrient excess to adipose insulin resistance.

RESULTS

Glucose is dispensable for insulin-responsive respiration

In this study, we sought to understand the role of glucose metabolism in adipose insulin resistance. We hypothesised that insulin resistance was caused by mitoROS generated from increased glucose metabolism. Since mitoROS is generated by enzymes that participate in mitochondrial respiration, we reasoned that glucose would fuel insulin-stimulated respiration to generate mitoROS. Thus, in the first instance, we examined the role of glucose in adipocyte respiration.

We delineated glucose metabolism from insulin action using galactose, a 'no glucose' sugar analogue previously shown to impair glycolysis (e.g., (15-17)). We confirmed that galactose ablated insulin-stimulated lactate production (Fig 1A). However, contrary to our hypothesis, insulin increased respiration (oxygen consumption in intact cells) both in the presence and absence of glucose (Fig 1B). In contrast, both glucose and insulin were required for maximal respiration, induced by a maximal dose of the mitochondrial uncoupler (BAM15). This suggests that insulin-dependent glucose metabolism can fuel respiration, but is not necessary for respiration under insulin-stimulated conditions.

One possibility is that insulin stimulates respiration by different mechanisms in the presence and absence of glucose. For instance, glucose utilisation may generate more reducing equivalents, increasing the proton gradient and respiration (increased respiration through increased supply). Alternatively, respiration would also increase in response to higher energy demand, which may manifest as a depleted proton gradient in the absence of glucose, if glucose is required for insulin-stimulated respiration. Thus, we examined

mitochondrial membrane potential (MMP), a surrogate for the proton gradient. Insulin did not alter MMP in the presence of glucose (p>0.05, two-way ANOVA comparing glucose ± insulin over time). Removing glucose led to a reduction in MMP (~2% difference between galactose/insulin versus glucose/insulin; p<0.01, two-way ANOVA). However, this change was mild in comparison to hypo- or hyperpolarisation observed with BAM15 and oligomycin, respectively (Fig 1C). This suggests that substrate supply and energy demand are synchronised in response to insulin, without significant energetic imbalance, even in the absence of glucose.

We next sought to translate our findings *ex vivo*. Since adipose tissue consists of various cell-types in addition to adipocytes (1), we tested whether glucose was required for respiration in mature adipocytes isolated from rat adipose tissue. We confirmed that galactose blunted insulin-responsive lactate levels (Fig 1D). With this tool, we found that insulin slightly increased respiration (Fig 1E), but this did not require glucose except in the presence of the mitochondrial uncoupler, FCCP (Fig 1F). Lower doses of FCCP had little effect on respiration (*data not shown*). Overall, this demonstrates that our findings in cultured adipocytes are conserved in primary adipocytes *ex vivo*.

Glucose only contributes a portion of respiration-derived CO_2

Given insulin could stimulate respiration without glucose, we predicted that glucose would not be a significant contributor to respiration-derived CO_2, i.e. CO_2 from pyruvate dehydrogenase (PDH) and the Krebs cycle. It is theoretically possible to calculate this from the JO_2 (respiration rate) if glucose is the sole substrate (18). However, there are other substrates present in our experiments, such as amino acids in the media and fatty acids from intracellular lipid stores. Each substrate varies in their respiratory quotient (CO_2 produced/O_2 consumed), rendering this approach challenging.

To overcome this, we measured JO_2 from cultured adipocytes using the XFp Extracellular Flux Analyzer (Seahorse Biosciences), which simultaneously measures the extracellular media acidification rate (ECAR) within the same experiment (Fig S1A). Importantly, ECAR is influenced by not only lactate production, but also bicarbonate formed by CO_2 production (18). We utilised this to calculate the contribution of glucose to cellular respiration (Fig 1G, detailed in the Experimental Procedures). Briefly, we used the buffering capacity of the media (Fig S1B) to convert the ECAR into the proton production rate. Next, we subtracted the lactate production rate from the proton production rate to obtain ECAR due to CO_2, from which we inferred the total CO_2 production (Fig 1H). Finally, we compared this value to the incorporation of (^{14}C-labelled) glucose into CO_2, determining that glucose contributes only 19.8% of respiration-derived CO_2 under insulin stimulation. These experiments were conducted in the presence of bicarbonate, which we have previously found to influence cellular respiration (14) In the absence of bicarbonate, we found a similar contribution of glucose to respiration-derived CO_2 (26.8%, *data not shown*).

Thus, glucose contributes a relatively minor portion of the oxidisable carbon for cellular respiration under insulin-stimulated conditions. Conversely, insulin can stimulate adipocyte respiration without glucose (Fig 1B,1F). Collectively, this suggests that glucose is dispensable for the increase in mitochondrial respiration upon insulin exposure.

Glucose is required for insulin-dependent mitoROS production

Since respiratory complexes also participate in mitoROS production (e.g., (19,20)), this raised the possibility that insulin treatment may similarly increase mitoROS levels independently of insulin-stimulated glucose metabolism. To maximise glucose oxidation, we utilised dichloroacetate (DCA), which causes the dephosphorylation of pyruvate dehydrogenase to promote the activity of this enzyme (21). Interestingly, although DCA rapidly decreased media acidification (Fig 2A), DCA treatment had little effect on global respiration (Fig 2B), even under maximal bioenergetic demand (BAM15). This provided further evidence that global respiration is not influenced by changes in glucose flux.

We treated adipocytes with insulin in the presence or absence of glucose and DCA. We initially utilised matrix-roGFP, a mitochondrially-targeted ROS-sensitive probe, which did not exhibit substantial changes in

signal upon treatment with either insulin or mPQ (Fig S2A-B). Subsequently, we assessed the dimer/monomer status of peroxiredoxin 3 (PRDX3) and PRDX2, which are robust, sensitive indicators of relative oxidant exposure in the mitochondria and cytosol, respectively (11). For instance, pre-treatment with antimycin A significantly increased PRDX3 dimerisation (Fig 2C, *first two lanes*; Fig 2D), but had a less pronounced effect on PRDX2 dimerisation (Fig 2C,D; $p \sim 0.060$ vs control, two-sample *t*-test) – this demonstrates that antimycin A more readily increases mitoROS, consistent with its known mechanism of action.

Insulin increased PRDX3 dimerisation, but only when glucose was present (Fig 2C,D). This was not due to an impairment of insulin signalling in the absence of glucose, as indicated by similar levels of phosphorylation of Akt kinase and its substrate, AS160 (Fig 2C,E). The insulin- and glucose-dependent increase in PRDX3 dimerisation was enhanced in the presence of DCA, which caused a sustained reduction in PDH phosphorylation throughout the time-course (Fig 2C,E). In contrast, the change in PRDX2 dimerisation was less consistent over time (Fig 2C,D). Overall, these data demonstrate that insulin increases mitoROS levels in a glucose-dependent manner.

Consequently, we examined the sensitivity of mitoROS to glucose uptake. As observed previously (21), glucose uptake increased with insulin and higher media glucose concentrations (Fig S2C). PRDX3 dimerisation also increased under these conditions (Fig 2F,G), particularly when physiological glucose concentrations (and the K_m of GLUT4 (22)) were reached. Inhibiting glucose uptake with cytochalasin B (Fig S2C) reduced PRDX3 dimerisation (Fig 2F,G) but did not affect respiration (Fig S2D). Furthermore, plotting PRDX3 dimerisation against glucose uptake in insulin-stimulated adipocytes revealed a sigmoidal trend (Fig 2H). This suggests that substantial PRDX3 dimerisation occurs once a threshold of glucose uptake is reached. Thus, mitoROS is sensitive to insulin-stimulated glucose uptake.

Glucose-dependent mitoROS does not cause insulin resistance

These data are consistent with the notion that glucose-dependent mitoROS is an endogenous signal to cause insulin resistance under conditions of excess nutrient supply (Fig 3A). If true, we would predict that sustained insulin exposure would increase glucose oxidation, mitoROS, and lead to acute insulin resistance. Furthermore, this would be exacerbated in the presence of DCA.

Thus, we exposed adipocytes to insulin, with or without DCA (Fig 3B). We included mPQ as a positive control for specifically increasing mitochondrial oxidant levels and causing insulin resistance (Fig S2E, (11)), and the thioreductase inhibitor, auranofin, as a control for PRDX3 dimerisation. MitoROS levels rose with prolonged insulin treatment (Fig 3C), and co-treatment with DCA and insulin increased mitoROS to a greater extent than observed with mPQ treatment (Fig 3C).

Since insulin-responsive GLUT4 trafficking is selectively impaired in adipocyte insulin resistance (23), we assessed insulin action by cell-surface glucose transporter activity (24,25). Contrary to our model (Fig 3A), we did not observe any detectable inhibition of insulin action by DCA treatment, with only mPQ causing insulin resistance within this acute time-frame (Fig 3D). This concurred with the presence of glucose and/or DCA having no consistent effect on insulin-stimulated signalling as measured by Akt and its substrate, AS160 (Fig 2C,E). Furthermore, in the presence of glucose, insulin rapidly stimulated GLUT4 translocation and the proportion of cell-surface GLUT4 did not decrease within 1 h (Fig 3E), which was a sufficient time-frame for glucose-dependent mitoROS levels to rise (Fig 2D). Thus, glucose-dependent mitoROS does not appear to cause acute insulin resistance.

MitoROS needs to increase before the insulin stimulus to impair insulin action

Although insulin-dependent glucose metabolism increases mitoROS levels higher than mPQ treatment (Fig 3C), mPQ was added prior to the insulin treatment (as in (11)). This would have allowed mitoROS to increase prior to the insulin stimulus, unlike glucose-dependent mitoROS (Fig 2C). Thus, mitoROS may need to increase prior to insulin stimulation to cause insulin resistance. To test this, we treated adipocytes with mPQ before or after insulin stimulation. Strikingly, mPQ pre-treatment impaired insulin-stimulated GLUT4 translocation (Fig 4A), but this was not

observed when cells were treated with mPQ after insulin stimulation (Fig 4B). However, in each case, mPQ increased mitoROS levels, assessed by PRDX3 dimerisation (Fig 4A,B). Thus, our data suggest that mitoROS only leads to insulin resistance if mitoROS increases prior to insulin stimulation (Fig 4C).

DISCUSSION

In this study, we examined the relationship between nutrient excess and insulin resistance in adipocytes. We tested the concept of 'glucose-dependent' insulin resistance, whereby insulin-stimulated glucose metabolism would fuel respiration, generate mitoROS, and feed back to reduce glucose uptake. Although insulin stimulated respiration in the absence of glucose (Fig 1), glucose was required for insulin to increase mitoROS (Fig 2). However, glucose-dependent mitoROS did not acutely cause insulin resistance (Fig 3) because mitoROS needed to increase before the insulin stimulus for insulin resistance to occur (Fig 4). This may explain why insulin-stimulated glucose utilisation does not acutely cause insulin resistance in adipocytes (Fig 4C).

Mitochondrial respiration is governed by nutrient supply and energy demand (12), permitting the mitochondrion to serve as a cellular sensor for energetic imbalance. Several observations suggest that for adipocytes exposed to insulin, respiration is driven by increased energy demand rather than substrate (glucose) supply. First, insulin stimulated respiration in both the absence or presence of glucose (Fig 1) and upon inhibition of glucose uptake (Fig S2D), and DCA treatment had no impact on respiration (Fig 3). Second, we previously showed that insulin stimulates anabolism before glucose uptake is maximal (24), corresponding with a transient decrease in the global energy charge in adipocytes. Here, we found that insulin treatment did not alter MMP (Fig 1), suggesting supply and demand are synchronised, hence respiration likely increases in response to the energetic demands of the cell. Third, although insulin stimulated glucose uptake by several fold (24), glucose only contributed a quarter of respiration-derived CO_2 upon insulin stimulation (Fig 1, S1). Finally, glucose only impacted respiration under maximal respiratory demand, whereby both insulin and glucose were required to increase further respiration in the presence of an uncoupler (Fig 1). Indeed, treatment with a mitochondrial uncoupler increased glucose oxidation substantially higher than insulin alone (21). Collectively, this suggests that insulin stimulates energy demand in adipocytes, but this increased demand is not enough to require substrate supply from exogenous glucose.

The minor contribution of glucose to respiration-derived CO_2 (Fig 1G) concurs with our previous tracer metabolomics analysis of insulin-stimulated adipocytes (24) – for instance, with insulin treatment, the unlabelled isotopologue of acetyl CoA was dominant, suggesting other carbon sources contributed substantially to the Krebs cycle. Given that insulin inhibits glycogen breakdown and lipolysis, this leaves amino acids as a potential respiratory substrate. Indeed, previous stable-isotope tracer studies that demonstrated that in adipocytes, the Krebs cycle can be fuelled by branched chain amino acids and glutamine (26,27). This provides a likely explanation for how insulin stimulated respiration in the absence of glucose (Fig 4C), by accessing carbon from amino acids for the Krebs cycle. Overall, these findings suggest that insulin plays a much larger role in directing cellular metabolism beyond stimulating glucose uptake, coordinating the oxidation of other substrates to fuel the energy demands of anabolism.

In contrast, glucose was specifically required for the insulin-stimulated increase in mitoROS, which was ablated by the absence of glucose or inhibition of glucose uptake, and accentuated by DCA treatment (Fig 2). Given that insulin suppresses lipid breakdown by anti-lipolysis, this together implies that the remaining substrates (e.g., amino acids in the DMEM buffer) do not contribute to insulin-stimulated oxidant production. Furthermore, PRDX3 dimerisation only increased when a threshold of glucose uptake was reached (Fig 2H), suggesting that mitoROS generated below this threshold can be adequately buffered by the adipocyte. Upon acute insulin stimulation, we speculate that sites of glucose-dependent mitoROS production would either be pyruvate dehydrogenase or mitochondrial glycerol 3-phosphate dehydrogenase (19,28), which represent more 'glucose-specific' sites of entry into mitochondrial respiration.

Collectively, these data demonstrate a disconnect between mitochondrial respiration and oxidant production (Fig 4C). Although both respiration and mitoROS generation occur in

the mitochondria, they differ in their substrate requirements, with only mitoROS levels increasing in the presence of glucose. Specifically, respiration responds to increases in energy demand, whereas mitoROS levels respond to increases in glucose supply. We believe that this disconnect between respiration and mitoROS enables adipocytes to distinguish between energetic demand and nutrient supply, finetuning its metabolism and insulin sensitivity to different nutritional and hormonal cues.

Although mitoROS are implicated in insulin resistance (8), glucose-dependent mitoROS did not acutely lead to insulin resistance (Fig 3). In contrast, treatment with mPQ in a similarly short time-frame was sufficient to induce insulin resistance (8). We subsequently found that mitoROS needed to increase prior to the insulin stimulus to induce insulin resistance (Fig 4). Although we cannot exclude the possibility that glucose oxidation and mPQ treatment generate different oxidant species and/or oxidants that arise from different cellular locations, our findings suggest that there is a temporal requirement for mitoROS to cause insulin resistance. Specifically, as mitoROS outweighs endogenous scavenging systems, the mitoROS likely reacts with a macromolecule required in the initial stages of insulin-stimulated glucose transport. Furthermore, since oxidative stress does not require long-term adaptive changes such as transcriptional modification to cause insulin resistance in adipocytes (29), it is likely to cause rapid changes in kinase signalling and/or GLUT4 trafficking. However, mitoROS did not affect Akt signalling (Fig 3), concurring with previous studies (11). Thus, it is tempting to speculate that mitoROS specifically blocks the insulin-dependent mobilisation of GLUT4 to the cell surface (e.g., exocytosis of GLUT4-containing vesicles), rather than steps involved in the maintenance of enhanced PM GLUT4 during an insulin stimulus, such as the recycling of PM GLUT4 via endosomes.

Teleologically, this temporal requirement for mitoROS suggests that the adipocyte needs to sense excess nutrient supply prior to the insulin stimulus in order to trigger insulin resistance. This is consistent with a model whereby consumption of a meal will not impair insulin action whereas oxidative stress upon chronic over-nutrition would lead to a persistent decrease in insulin action. This raises the question, what physiological substrate(s) are oxidised to cause oxidant-induced insulin resistance (Fig 4C)? One strong candidate are fatty acids, since fatty acid oxidation has been demonstrated to impair insulin-stimulated glucose uptake in myotubes, and muscle tissue in rodents and human subjects (e.g., (6,30,31)). Also, insulin suppresses lipolysis – conversely, fatty acid oxidation would be elevated when insulin levels are low, providing a source of mitoROS prior to an insulin stimulus. This may explain why both long-term fasting (sustained lipolysis) and Western diets (high fat) both cause insulin resistance, in isolated rat adipocytes (32-35) and at the whole-body level (reviewed in (8)). Ultimately, this would mechanistically link nutrient excess with insulin resistance.

EXPERIMENTAL PROCEDURES

Reagents

The following chemicals were used in this study: insulin (Sigma-Aldrich #I5500), dichloroacetate (sodium salt, Sigma-Aldrich #347795), oligomycin (Sigma-Aldrich #O4876), rotenone (Sigma-Aldrich #R8875), antimycin A (Sigma-Aldrich #A8674), and cytochalasin B (Sigma-Aldrich #C6762). In addition, BAM15 (36) was a gift from Dr Kyle Hoehn (The University of New South Wales, Sydney, Australia) and mPQ (37) was a gift from Dr Mike Murphy (University of Cambridge, Cambridge, United Kingdom). Matrix-roGFP was a gift from Paul Schumacker (Addgene plasmid #49437; http://n2t.net/addgene:49437; RRID:Addgene_49437).

Cell culture

3T3-L1 fibroblasts were cultured as described previously (38), using Media A, consisting of bicarbonate-buffered DMEM (Life Technologies, #11960), supplemented with 10% (v/v) foetal bovine serum (Life Technologies, #16000044) and 2 mM GlutaMAX (Life Technologies, #35050061). 3T3-L1 fibroblasts were differentiated into adipocytes as described previously (24,38). Adipocytes were used between days 9-12 after the initiation of differentiation. At least 90% of the cells were differentiated prior to experiments. These cells were routinely tested for mycoplasma infection.

Unless otherwise specified, prior to insulin stimulation treatments, cells were

serum-starved for at least 2 h. This involved washing cells three times with PBS and incubating them in basal media. By default, the basal media was Media B, which consisted of bicarbonate-buffered DMEM (Life Technologies #11960), supplemented with 0.2% (w/v) bovine serum albumin (BSA, Bovostar) and 2 mM GlutaMAX.

For experiments within the CO_2 incubator that involved treatment with different sugars, cells were washed twice after serum-starvation: once with PBS, then with BSF-DMEM, which consisted of substrate-free DMEM (Sigma #D5030), supplemented with 44 mM $NaHCO_3$ and adjusted to pH 7.4 with CO_2 (dry ice). Cells were then incubated in Media BS, which consisted of BSF-DMEM, supplemented with 0.2% (w/v) BSA, 1 mM GlutaMAX, 1 mM glutamine, and sugar (glucose/galactose) as specified in the figure legends. The supplementation of glutamine in addition to GlutaMAX served to provide an immediate source of glutamine substrate for experiments involving early time-points.

For metabolic assays performed outside of the CO_2 incubator, cells were washed twice after serum-starvation: once with PBS, then with HSF-DMEM, which consisted of substrate-free DMEM (Sigma-Aldrich #D5030) supplemented with 30 mM Na-HEPES (pH 7.4) and adjusted to pH 7.4 with NaOH. Cells were then incubated in Media C, which consisted of HSF-DMEM, supplemented with 0.2% (w/v) BSA, 1 mM $NaHCO_3$ (added fresh), 1 mM glutamine, 1 mM GlutaMAX, and sugars (glucose/galactose) as specified in the figure legends. Alternatively, cells were assayed in Media CX, which consisted of Media C without BSA, as specified in the figure legends.

Quantification of lactate content

Lactate content was assayed enzymatically using the hydrazine sink method, as described previously (21,39).

Quantification of glucose uptake

Glucose uptake was determined by measuring the disappearance of media glucose, as described previously (21,24). This differs from the measurement of glucose transport, which is described below.

Respirometry using the XFp Analyzer (Seahorse BioSciences)

On Day 7-8 of differentiation, 3T3-L1 adipocytes were seeded onto XFp plates described previously (14). Cells were prepared for the assay as described previously (14), with minor modifications. Specifically, cells were washed 4 times with PBS before incubation in Media C, supplemented with 25 mM glucose, for at least 1.5 h in a non-CO_2 incubator at 37 °C. Cells were then washed once with PBS, once with HSF-DMEM, and incubated in Media CX (150 µl/well), supplemented with 25 mM sugar (glucose/galactose). Cells were then assayed in the XFp Analyzer: following a 12 min equilibration period, respiration and extracellular acidification rates were measured with mix/wait/read cycles of 3/0/2 min. Following stabilisation of baseline rates, compounds were injected sequentially as indicated in the figures. Flux rates were normalised to cellular DNA content, the latter being quantified as described below.

Measurement of mitochondrial membrane potential

Mitochondrial membrane potential was assessed using the 'quenching method' with tetramethylrhodamine methyl ester (TMRM) dye (40). 3T3-L1 adipocytes were seeded into black 96-well plates (Corning), pre-coated with Matrigel (Corning), in a similar manner as seeding into XFp plates (above). On the day of the experiment, cells were washed 4 times with PBS (150 µl per wash) before incubation in Media C, supplemented with 25 mM glucose, for at least 1.5 h in a non-CO_2 incubator at 37 °C. In the last 30 min of this serum starvation period, cells were labelled with 500 nM TMRM (or DMSO control – 'TMRM-free').

Cells were then washed twice with PBS, once with HSF-DMEM, then incubated in 90 µl Media CX per well. The plate was incubated at 37 °C in the FLUOstar Omega microplate reader (BMG Labtech). Fluorescence was measured every 90 s using the top optic at 544 nm excitation and 590 nm emission, with 20 flashes per well. This pre-read period was conducted for 15 min to ensure a stable baseline measurement was achieved for each well. Drugs were added in the following sequence in 10 µl, followed by fluorescence measurement (with final drug concentrations and treatment times indicated in the figure): glucose or galactose; insulin or naïve media control; oligomycin, BAM15, or DMSO control.

At the end of the experiment, aliquots of media were taken from the wells treated with DMSO (i.e., glucose/galactose, insulin/control) and assessed for lactate content (described above) to check that insulin and sugar responses were similar to Fig. 1A (*data not shown*).

Fluorescence measurements were first adjusted by the fluorescence of identically-treated cell-free and TMRM-free controls, to account for background fluorescence. Next, measurements were normalised to the last measurement of the pre-read period, to account for well-to-well differences in TMRM labelling. Finally, these values were normalised to the glucose-control-DMSO condition, to account for changes in signal independent of drug treatments. This normalised measurement was denoted 'relative TMRM signal'.

Measurement of glucose oxidation and PPP flux

Following serum-starvation in Media B, cells were incubated with Media C supplemented with 10 mM glucose, and either 0.5 µCi/ml [1-^{14}C]-, 1 µCi/ml [6-^{14}C]-, or 1 µCi/ml [U-^{14}C]-glucose tracer. Following the addition of drug treatments, glucose oxidation was assessed as described previously (13,21) – briefly, a gas-trap was installed in each well, plates were sealed, and following treatment cells were quenched by acidification. Radioactivity of the gas-trapping solution was measured by liquid scintillation counting and adjusted to cell-free controls.

Total glucose oxidation was derived from the use of [U-^{14}C]-glucose tracer and PPP flux was derived from the use of [1-^{14}C]- and [6-^{14}C]-glucose tracers (41,42). Calculating PPP flux also required the rate of glucose uptake and protein content, which were derived from cells treated in parallel (in the absence of radiolabel or gas-trap installed). Glucose uptake was determined as described above, and protein content was determined as described below after washing cells thrice with ice-cold PBS and lysis in PBS containing 1% (v/v) Triton X-100.

Assessment of insulin action by glucose transporter activity

Glucose transporter activity was measured as described previously (24). Briefly, following treatment, cells were washed with ice-cold PBS, incubated in cold Krebs-Ringer phosphate buffer (24) without any drugs, and assessed for 2-deoxyglucose uptake on ice. These cold conditions ensured the rate of uptake was solely dependent on the membrane trafficking, and movement of glucose transporters to the cell surface, that had occurred during the treatment period (but not the 2-deoxyglucose uptake period).

Assessment of insulin action by GLUT4 translocation

GLUT4 translocation in 3T3-L1 adipocytes was measured as described previously (11). Briefly, 3T3-L1 fibroblasts were retrovirally-infected with a construct expressing HA-tagged GLUT4, differentiated, and seeded into black 96-well plates. Following treatment, the quantity of cell-surface HA was assessed by immunofluorescence staining and normalised to total HA content (11).

Normalisation for cell culture experiments

Flux rates were normalised to cellular protein or DNA content, using cell lysate derived from the respective assay or from cells treated in parallel. Unless otherwise specified, flux rates were normalised to protein content, determined using the Pierce bicinchoninic acid assay kit (ThermoFisher) according to the manufacturer's instructions. If flux rates were normalised to DNA, the DNA quantification was performed following cell lysis by repeated freeze-thaw, using Hoechst staining as described previously (21).

Western blotting

Following treatment, cells were harvested for protein and lysates subjected to Western blotting as described previously (11). Antibodies detecting pS473-Akt (clone 587F11, catalog #4051), pT308-Akt (catalog #9275), Akt (clone 11E7, catalog #4685), and pT642-AS160 (catalog #4288) were obtained from Cell Signaling Technology. The antibodies detecting PDH-E1α (clone H-131, catalog #sc292543) and 14-3-3 (clone K-19, catalog #sc-629) was obtained from Santa Cruz Biotechnology. The antibody detecting pS293-PDH-E1α (catalog #ABS204) was obtained from Millipore. The antibody detecting PRDX3 (catalog #LF-PA0030) was obtained from Life Technologies. The antibody detecting PRDX2 (clone EPR5154, catalog #ab109367) was obtained from Abcam. Densitometric analysis was performed either using Fiji software (43) or LICOR Image Studio.

Assessment of mitochondrial oxidative stress by microscopy

3T3-L1 adipocytes were electroporated and imaged as described previously (44). On Day 7 of differentiation, 3T3-L1 adipocytes were tryspinised, pelleted at 150 g for 5 min, and washed 3 times with PBS before resuspension in electroporation solution (20 mM HEPES, 135 mM KCl, 2 mM $MgCl_2$, 0.5% (w/v) Ficoll 400, 1% (v/v) DMSO, 2 mM ATP and 5 mM glutathione, pH 7.6) and 5 µg of plasmid DNA (matrix-roGFP). Cells were then electroporated at 200 mV for 20 ms and plated onto Matrigel-coated 35 mm Ibidi glass-bottom m-Dishes dishes.

Imaging experiments were performed 24 h post-electroporation. Cells were serum-starved in Media B and imaged in Fluorobrite DMEM (Life Technologies), supplemented with 0.2% (w/v) BSA and 2 mM GlutaMAX, under 10% CO_2. Imaging was performed on a Nikon Ti inverted microscope equipped with a Spectral Applied Research Diskovery spinning disk module and an Okolab cage incubator maintained at 37 °C. Drugs were added using a custom-made perfusion system. Image analysis was performed in Fiji (43) using a scripted analysis pipeline.

Quantification of the contribution of glucose to respiration-derived CO_2

Our approach (Fig 1G) was based on the principle that ECAR is influenced by both lactate production and bicarbonate derived from CO_2 release (18). This required several sets of flux data (ECAR, lactate production, and glucose oxidation), each derived from separate batches of cells. These flux parameters, when measured in insulin-stimulated 3T3-L1 cells (in Media C), typically varied by <20% between batches of cells (*data not shown*).

To quantify the contribution of glucose to respiration-derived CO_2, the following steps were performed:

(i) The total ECAR (mpH/h) was derived from flux data (e.g., Fig S1A). Since ECAR initially rises before reaching a plateau with insulin treatment, total ECAR was determined by calculating the area-under-the-curve using the trapezoidal rule. Since maximal ECAR remains constant for at least an hour after insulin stimulation (*data not shown*), ECAR flux was extrapolated to 1 h using the last three timepoints at the maximal rate if complete data was not available.

(ii) The buffering capacity (BF) of the media (Fig S1B) was determined by incubating naïve media in the Seahorse XFp and measuring pH changes following repeated injections of 1 M NaOH or HCl. Close to the pKa, the buffering curve is 'pseudo-linear' (18) and thus the gradient can be used to determine buffering capacity (µM H^+/mpH, i.e. change in $[H^+]$ per change in pH).

(iii) The proton production rate (PPR, changes in media $[H^+]$ in an XFp well) was determined from the ECAR (changes in media pH), using the media buffering capacity, measurement chamber volume, and K_{vol} adjustment factor (45):

$$\text{PPR (pmol } H^+/h) = \text{ECAR (mpH/h)} \cdot \text{BF } (\mu M\ H^+/\text{mpH}) \cdot \text{volume (2.28 µl)} \cdot K_{vol} \quad (1.19)$$

(iv) Next, we obtained lactate production data (21), which involved 3T3-L1 cells treated with 100 nM insulin for 1 h in Media C, supplemented 25 mM glucose. The cells were treated under slightly different conditions (e.g., plate format, presence of BSA in assay media), but these parameters did not impact insulin-stimulated lactate production (Fig S1C). The lactate production data was scaled down to the cell number in a well of an XFp plate.

(v) Bicarbonate production was determined from the PPR and lactate production data. Since each lactate molecule is effluxed with 1 proton and the conversion of CO_2 into $NaHCO_3$ generates 1 proton, these outputs are stoichiometrically 1-to-1 with PPR. Thus, we calculated bicarbonate production as the difference between PPR and lactate production:

$$NaHCO_3 \text{ production (pmol } H^+/h) = \text{PPR (pmol } H^+/h) - \text{lactate production (pmol } H^+/h)$$

We assumed that other sources of proton efflux were negligible (18).

(vi) Total CO_2 production was determined from bicarbonate production by accounting for the solubility of bicarbonate in water (18).

(vii) The contribution of glucose to CO_2 production was calculated using measurements of the incorporation of ^{14}C-radiolabelled glucose into CO_2 (21). Briefly, 3T3-L1 cells were treated with 100 nM insulin for 1 h in Media C, supplemented with 25 mM glucose and [U-^{14}C]-glucose tracer. This value was scaled down to the cell number in a well of

an XFp plate, and multiplied by 6 (1 glucose generates 6 CO_2) to obtain the production rate of glucose-derived CO_2.

(viii) Since CO_2 can be generated by the pentose phosphate pathway (PPP) in addition to respiration, we compared the incorporation of glucose into CO_2 versus PPP flux (Fig S1D). PPP flux was stimulated by insulin and abolished with an inhibitor of 6-phosphogluconate dehydrogenase, 6-aminonicotinamide (Fig S1D). Nevertheless, PPP-derived CO_2 was negligible compared to the total incorporation of glucose into CO_2 (performed in parallel, Fig S1D), considering that PPP generates 1 CO_2 per glucose molecule compared to 6 CO_2 via respiration. Thus, it was assumed that glucose-derived CO_2 was solely derived from respiration.

(ix) Glucose-derived CO_2 production was compared to total CO_2 production, yielding the contribution of glucose to respiration-derived CO_2.

Metabolic assays in primary adipocytes

Isolation and assay buffers

Buffers included Krebs-Henseleit buffer (KHB: 120 mM NaCl, 4.7 mM KCl, 1.18 mM KH_2PO_4, 1.17 mM $MgSO_4$, 1.8 mM $CaCl_2$, 30 mM Na-HEPES, 1 mM $NaHCO_3$ (added fresh), 1% (w/v) fatty-acid-free BSA (Sigma), pH adjusted to 7.4 with NaOH), KHB-Glc buffer (KHB, supplemented with 10 mM glucose), and assay buffer (HSF-DMEM, supplemented with 1 mM $NaHCO_3$ (added fresh), 1 mM glutamine, 1 mM GlutaMAX, and 1% (w/v) fatty-acid-free BSA, with pH adjusted to 7.4 with NaOH). All buffers were maintained at 37 °C throughout the experiment.

Isolation of mature primary adipocytes

Male Sprague Dawley rats were housed at 23 °C in individually ventilated cages on a 12-hour light:dark cycle with *ad libitum* access to standard rodent chow and water. Rat experiments were approved by the University of Sydney Animal Ethics Committee (project #2018/1418). At 7-8 weeks of age (200-300 g), rats were sacrificed with CO_2. Mature primary adipocytes were isolated, as described previously (21). Briefly, epididymal fat pads were isolated and collagenase-digested in KHB-Glc buffer. The isolated adipocytes were washed twice with KHB and then twice with assay buffer, to remove collagenase, non-adipocyte cells, and glucose from the digestion buffer. After the final wash, the infranatant was removed and aliquots of adipocyte suspension were used in the assays below.

Respirometry of primary adipocytes using the O2k oxygraph (Oroboros)

High resolution oxygen consumption measurements were conducted using the O2K oxygraph (series H). 200-400 µl of primary adipocyte suspension were loaded into each O2K chamber, made up to a final volume of 2.1 ml with assay media supplemented with a (final concentration) of 5 mM glucose or galactose. Experiments were conducted at 37 °C with stirring at 750 rpm stirring and data recording at 2 s intervals. Cells were allowed to equilibrate prior to the sequential addition of pharmacological agents as indicated in the figure legends. Respiratory flux data was analysed using DatLab 7.3.0.3 (Oroboros).

Following the experiment, aliquots (3x 500 µl) of cell suspension were taken from each chamber and immediately frozen. DNA was isolated under high salt conditions with organic extraction, similar in principle to what has been described previously (21). After the addition of 0.2 vol of 5 M NaCl and mixing, an equal volume (600 µl) of $CHCl_3$ was added. Samples were mixed thoroughly and centrifuged for 20 min at 16,000 x *g* and 4 °C. The supernatant was assayed for DNA content using SyBr stain (Life Technologies), according to the manufacturer's instructions. Fluorescence measurements were compared to a standard curve of salmon sperm DNA, spiked with naïve assay buffer extracted alongside adipocyte samples. Furthermore, extraction efficiency was determined by spiking one aliquot of adipocyte suspension from each O2K chamber (out of three) with salmon sperm DNA prior to extraction.

Respiration fluxes were normalised to DNA content and then to the baseline respiration of the chamber receiving the glucose + insulin condition.

Lactate measurement in primary adipocytes

Adipocytes were assessed for lactate production as described previously (21), with slight modifications. Briefly, 200 µl of adipocyte suspension was dispensed into wells of 24-well polystyrene, tissue culture microplates (Corning). To each well, 50 µl of pre-warmed assay buffer containing glucose or galactose, and PBS control or insulin, was added. As a result, each well contained a final

volume of 250 µl, with 5 mM sugar and either PBS control or 20 nM insulin. Plates were then immediately sealed with TopSeal-A PLUS (PerkinElmer) and gently rocked for 1 h with a rocking platform in a 37 °C incubator.

Following incubation, cells were immediately quenched by the addition of 400 µl MeOH, followed by 400 µl water. Lysates were transferred to tubes, 800 µl $CHCl_3$ was added, and samples were vortexed briefly prior to centrifugation for 20 min at 16,000 x *g* and 4 °C. The supernatant was lyophilised using an EZ-2 centrifugal evaporator (GeneVac), resuspended in water, and assayed for lactate content enzymatically as described above and previously (21).

ACKNOWLEDGEMENTS

The authors would like to thank the Charles Perkins Centre (CPC) Research Support team, particularly Dr Ian Garthwaite, Dr Natalia Magarinos, Mr Harry Simpson, Dr Melissa Gardiner, and Dr Macarena Rodriguez, for technical support. DEJ was supported by a National Health and Medical Research Council (NHMRC) Senior Principal Research Fellowship (APP1019680) and NHMRC project grants (GNT1061122, GNT1086851). GJC was supported by a Professorial Research Fellowship from the University of Sydney Medical School. DEJ and GJC were also supported by an NHMRC project grant (GNT1086850). JRK was funded by an NHMRC Early Career Fellowship (APP1072440), Australian Diabetes Society Skip Martin Early-Career Fellowship, Diabetes Australia Research Program grant, and CPC Early-Career Seed Funding grant. DJF was funded by Medical Research Council Career Development Award (MR/S007091/1). The contents of the published material are solely the responsibility of the authors and do not reflect the views of the NHMRC.

CONFLICTS OF INTEREST

The authors declare that they have no conflicts of interest with the contents of this article.

AUTHOR CONTRIBUTIONS

Conceptualisation: JRK, DJF, DEJ; Formal analysis: JRK; Funding acquisition: JRK, GJC, DJF, DEJ; Investigation: JRK, SDE, AD-V, KCC, JGB, DJF; Methodology: JRK, KHF-W; Supervision: GJC, DJF, DEJ; Writing – original draft: JRK, DJF, DEJ; Writing – review & editing: all authors

REFERENCES

1. Rosen, E. D., and Spiegelman, B. M. (2014) What we talk about when we talk about fat. *Cell* **156**, 20-44
2. Garvey, W. T., and Kolterman, O. G. (1988) Correlation of in vivo and in vitro actions of insulin in obesity and noninsulin-dependent diabetes mellitus: role of the glucose transport system. *Diabetes Metab Rev* **4**, 543-569
3. Kraegen, E. W., Clark, P. W., Jenkins, A. B., Daley, E. A., Chisholm, D. J., and Storlien, L. H. (1991) Development of muscle insulin resistance after liver insulin resistance in high-fat-fed rats. *Diabetes* **40**, 1397-1403
4. Turner, N., Kowalski, G. M., Leslie, S. J., Risis, S., Yang, C., Lee-Young, R. S., Babb, J. R., Meikle, P. J., Lancaster, G. I., Henstridge, D. C., White, P. J., Kraegen, E. W., Marette, A., Cooney, G. J., Febbraio, M. A., and Bruce, C. R. (2013) Distinct patterns of tissue-specific lipid accumulation during the induction of insulin resistance in mice by high-fat feeding. *Diabetologia* **56**, 1638-1648
5. Abel, E. D., Peroni, O., Kim, J. K., Kim, Y. B., Boss, O., Hadro, E., Minnemann, T., Shulman, G. I., and Kahn, B. B. (2001) Adipose-selective targeting of the GLUT4 gene impairs insulin action in muscle and liver. *Nature* **409**, 729-733
6. Hoehn, K. L., Salmon, A. B., Hohnen-Behrens, C., Turner, N., Hoy, A. J., Maghzal, G. J., Stocker, R., Van Remmen, H., Kraegen, E. W., Cooney, G. J., Richardson, A. R., and James, D. E. (2009) Insulin resistance is a cellular antioxidant defense mechanism. *Proc Natl Acad Sci U S A* **106**, 17787-17792
7. Fazakerley, D. J., Chaudhuri, R., Yang, P., Maghzal, G. J., Thomas, K. C., Krycer, J. R., Humphrey, S. J., Parker, B. L., Fisher-Wellman, K. H., Meoli, C. C., Hoffman, N. J., Diskin, C., Burchfield, J. G., Cowley, M. J., Kaplan, W., Modrusan, Z., Kolumam, G., Yang, J. Y., Chen, D. L., Samocha-Bonet, D., Greenfield, J. R., Hoehn, K. L., Stocker, R., and James, D. E. (2018) Mitochondrial CoQ deficiency is a common driver of mitochondrial oxidants and insulin resistance. *Elife* **7**, e32111
8. Fazakerley, D. J., Krycer, J. R., Kearney, A. L., Hocking, S. L., and James, D. E. (2018) Muscle and adipose tissue insulin resistance: malady without mechanism? *J Lipid Res*
9. Montgomery, M. K., and Turner, N. (2015) Mitochondrial dysfunction and insulin resistance: an update. *Endocr Connect* **4**, R1-R15

10. De Pauw, A., Tejerina, S., Raes, M., Keijer, J., and Arnould, T. (2009) Mitochondrial (dys)function in adipocyte (de)differentiation and systemic metabolic alterations. *Am J Pathol* **175**, 927-939
11. Fazakerley, D. J., Minard, A. Y., Krycer, J. R., Thomas, K. C., Stockli, J., Harney, D. J., Burchfield, J. G., Maghzal, G. J., Caldwell, S. T., Hartley, R. C., Stocker, R., Murphy, M. P., and James, D. E. (2018) Mitochondrial oxidative stress causes insulin resistance without disrupting oxidative phosphorylation. *J Biol Chem* **293**, 7315-7328
12. Fisher-Wellman, K. H., and Neufer, P. D. (2012) Linking mitochondrial bioenergetics to insulin resistance via redox biology. *Trends Endocrinol Metab* **23**, 142-153
13. Krycer, J. R., Diskin, C., Nelson, M. E., Zeng, X. Y., Fazakerley, D. J., and James, D. E. (2018) A gas trapping method for high-throughput metabolic experiments. *Biotechniques* **64**, 27-29
14. Krycer, J. R., Fisher-Wellman, K. H., Fazakerley, D. J., Muoio, D. M., and James, D. E. (2017) Bicarbonate alters cellular responses in respiration assays. *Biochem Biophys Res Commun* **489**, 399-403
15. Eagle, H., Barban, S., Levy, M., and Schulze, H. O. (1958) The utilization of carbohydrates by human cell cultures. *J Biol Chem* **233**, 551-558
16. Reitzer, L. J., Wice, B. M., and Kennell, D. (1979) Evidence that glutamine, not sugar, is the major energy source for cultured HeLa cells. *J Biol Chem* **254**, 2669-2676
17. Chang, C. H., Curtis, J. D., Maggi, L. B., Jr., Faubert, B., Villarino, A. V., O'Sullivan, D., Huang, S. C., van der Windt, G. J., Blagih, J., Qiu, J., Weber, J. D., Pearce, E. J., Jones, R. G., and Pearce, E. L. (2013) Posttranscriptional control of T cell effector function by aerobic glycolysis. *Cell* **153**, 1239-1251
18. Mookerjee, S. A., Gerencser, A. A., Nicholls, D. G., and Brand, M. D. (2017) Quantifying intracellular rates of glycolytic and oxidative ATP production and consumption using extracellular flux measurements. *J Biol Chem* **292**, 7189-7207
19. Brand, M. D. (2010) The sites and topology of mitochondrial superoxide production. *Exp Gerontol* **45**, 466-472
20. Quinlan, C. L., Perevoshchikova, I. V., Hey-Mogensen, M., Orr, A. L., and Brand, M. D. (2013) Sites of reactive oxygen species generation by mitochondria oxidizing different substrates. *Redox Biol* **1**, 304-312
21. Krycer, J. R., Quek, L. E., Francis, D., Fazakerley, D. J., Elkington, S. D., Diaz-Vegas, A., Cooke, K. C., Weiss, F. C., Duan, X., Kurdyukov, S., Zhou, P. X., Tambar, U. K., Hirayama, A., Ikeda, S., Kamei, Y., Soga, T., Cooney, G. J., and James, D. E. (2019) Lactate production is a prioritized feature of adipocyte metabolism. *J Biol Chem*, in press
22. Palfreyman, R. W., Clark, A. E., Denton, R. M., Holman, G. D., and Kozka, I. J. (1992) Kinetic resolution of the separate GLUT1 and GLUT4 glucose transport activities in 3T3-L1 cells. *Biochem J* **284 (Pt 1)**, 275-282
23. Tan, S. X., Fisher-Wellman, K. H., Fazakerley, D. J., Ng, Y., Pant, H., Li, J., Meoli, C. C., Coster, A. C., Stockli, J., and James, D. E. (2015) Selective insulin resistance in adipocytes. *J Biol Chem* **290**, 11337-11348
24. Krycer, J. R., Yugi, K., Hirayama, A., Fazakerley, D. J., Quek, L. E., Scalzo, R., Ohno, S., Hodson, M. P., Ikeda, S., Shoji, F., Suzuki, K., Domanova, W., Parker, B. L., Nelson, M. E., Humphrey, S. J., Turner, N., Hoehn, K. L., Cooney, G. J., Soga, T., Kuroda, S., and James, D. E. (2017) Dynamic Metabolomics Reveals that Insulin Primes the Adipocyte for Glucose Metabolism. *Cell Rep* **21**, 3536-3547
25. Tan, S. X., Ng, Y., and James, D. E. (2010) Akt inhibitors reduce glucose uptake independently of their effects on Akt. *Biochem J* **432**, 191-197
26. Green, C. R., Wallace, M., Divakaruni, A. S., Phillips, S. A., Murphy, A. N., Ciaraldi, T. P., and Metallo, C. M. (2016) Branched-chain amino acid catabolism fuels adipocyte differentiation and lipogenesis. *Nat Chem Biol* **12**, 15-21
27. Liu, L., Shah, S., Fan, J., Park, J. O., Wellen, K. E., and Rabinowitz, J. D. (2016) Malic enzyme tracers reveal hypoxia-induced switch in adipocyte NADPH pathway usage. *Nat Chem Biol* **12**, 345-352

28. Wong, H. S., Dighe, P. A., Mezera, V., Monternier, P. A., and Brand, M. D. (2017) Production of superoxide and hydrogen peroxide from specific mitochondrial sites under different bioenergetic conditions. *J Biol Chem* **292**, 16804-16809
29. Chaudhuri, R., Krycer, J. R., Fazakerley, D. J., Fisher-Wellman, K. H., Su, Z., Hoehn, K. L., Yang, J. Y. H., Kuncic, Z., Vafaee, F., and James, D. E. (2018) The transcriptional response to oxidative stress is part of, but not sufficient for, insulin resistance in adipocytes. *Sci Rep* **8**, 1774
30. Dresner, A., Laurent, D., Marcucci, M., Griffin, M. E., Dufour, S., Cline, G. W., Slezak, L. A., Andersen, D. K., Hundal, R. S., Rothman, D. L., Petersen, K. F., and Shulman, G. I. (1999) Effects of free fatty acids on glucose transport and IRS-1-associated phosphatidylinositol 3-kinase activity. *J Clin Invest* **103**, 253-259
31. Hoy, A. J., Brandon, A. E., Turner, N., Watt, M. J., Bruce, C. R., Cooney, G. J., and Kraegen, E. W. (2009) Lipid and insulin infusion-induced skeletal muscle insulin resistance is likely due to metabolic feedback and not changes in IRS-1, Akt, or AS160 phosphorylation. *Am J Physiol Endocrinol Metab* **297**, E67-75
32. Thacker, S. V., Nickel, M., and DiGirolamo, M. (1987) Effects of food restriction on lactate production from glucose by rat adipocytes. *Am J Physiol* **253**, E336-342
33. Newby, F. D., Sykes, M. N., and DiGirolamo, M. (1988) Regional differences in adipocyte lactate production from glucose. *Am J Physiol* **255**, E716-722
34. Newby, F. D., Wilson, L. K., Thacker, S. V., and DiGirolamo, M. (1990) Adipocyte lactate production remains elevated during refeeding after fasting. *Am J Physiol* **259**, E865-871
35. Bernstein, R. S., Zimmerman, K. S., and Carney, A. L. (1981) Absence of impaired glucose utilization in adipocytes from rats fed a carbohydrate-free, high protein diet. *J Nutr* **111**, 237-243
36. Kenwood, B. M., Weaver, J. L., Bajwa, A., Poon, I. K., Byrne, F. L., Murrow, B. A., Calderone, J. A., Huang, L., Divakaruni, A. S., Tomsig, J. L., Okabe, K., Lo, R. H., Cameron Coleman, G., Columbus, L., Yan, Z., Saucerman, J. J., Smith, J. S., Holmes, J. W., Lynch, K. R., Ravichandran, K. S., Uchiyama, S., Santos, W. L., Rogers, G. W., Okusa, M. D., Bayliss, D. A., and Hoehn, K. L. (2014) Identification of a novel mitochondrial uncoupler that does not depolarize the plasma membrane. *Mol Metab* **3**, 114-123
37. Robb, E. L., Gawel, J. M., Aksentijevic, D., Cocheme, H. M., Stewart, T. S., Shchepinova, M. M., Qiang, H., Prime, T. A., Bright, T. P., James, A. M., Shattock, M. J., Senn, H. M., Hartley, R. C., and Murphy, M. P. (2015) Selective superoxide generation within mitochondria by the targeted redox cycler MitoParaquat. *Free Radic Biol Med* **89**, 883-894
38. Fazakerley, D. J., Naghiloo, S., Chaudhuri, R., Koumanov, F., Burchfield, J. G., Thomas, K. C., Krycer, J. R., Prior, M. J., Parker, B. L., Murrow, B. A., Stockli, J., Meoli, C. C., Holman, G. D., and James, D. E. (2015) Proteomic Analysis of GLUT4 Storage Vesicles Reveals Tumor Suppressor Candidate 5 (TUSC5) as a Novel Regulator of Insulin Action in Adipocytes. *J Biol Chem* **290**, 23528-23542
39. Prabhu, A. V., Krycer, J. R., and Brown, A. J. (2013) Overexpression of a key regulator of lipid homeostasis, Scap, promotes respiration in prostate cancer cells. *FEBS Lett* **587**, 983-988
40. Perry, S. W., Norman, J. P., Barbieri, J., Brown, E. B., and Gelbard, H. A. (2011) Mitochondrial membrane potential probes and the proton gradient: a practical usage guide. *Biotechniques* **50**, 98-115
41. Katz, J., and Wood, H. G. (1963) The use of C14O2 yields from glucose-1- and -6-C14 for the evaluation of the pathways of glucose metabolism. *J Biol Chem* **238**, 517-523
42. Ashcroft, S. J., Weerasinghe, L. C., Bassett, J. M., and Randle, P. J. (1972) The pentose cycle and insulin release in mouse pancreatic islets. *Biochem J* **126**, 525-532
43. Schindelin, J., Arganda-Carreras, I., Frise, E., Kaynig, V., Longair, M., Pietzsch, T., Preibisch, S., Rueden, C., Saalfeld, S., Schmid, B., Tinevez, J. Y., White, D. J., Hartenstein, V., Eliceiri, K., Tomancak, P., and Cardona, A. (2012) Fiji: an open-source platform for biological-image analysis. *Nat Methods* **9**, 676-682

44. Norris, D. M., Yang, P., Krycer, J. R., Fazakerley, D. J., James, D. E., and Burchfield, J. G. (2017) An improved Akt reporter reveals intra- and inter-cellular heterogeneity and oscillations in signal transduction. *J Cell Sci* **130**, 2757-2766
45. Romero, N., Swain, P., Neilson, A., and Dranka, B. P. (2017) Improving Quantification of Cellular Glycolytic Rate Using Agilent Seahorse XF Technology. *Agilent Technologies Application Note*

FIGURE LEGENDS

Figure 1. Glucose is dispensable for insulin-stimulated respiration in adipocytes. ***A***, 3T3-L1 adipocytes were treated for 1 h with or without 100 nM insulin (Ins) in Media BS, supplemented with 25 mM glucose (Glc) or galactose (Gal). Following treatment, lactate production was quantified enzymatically as described in the Experimental Procedures. Data presented as mean + SEM, from 3 separate experiments. ***B***, 3T3-L1 adipocytes were incubated in Media CX supplemented with 25 mM Glc or Gal, and cellular respiration (JO_2) was measured using the XFp Analyzer following sequential treatment with (or without) Ins (100 nM), oligomycin (Oligo, 10 µg/ml), BAM15 (10 µM), rotenone (Rot, 5 µM), and antimycin A (AA, 10 µM) at the time-points indicated. Data presented as mean ± SEM, from 4 separate experiments. ***C***, 3T3-L1 adipocytes were pre-loaded with TMRM dye, and fluorescence was measured following incubation in Media CX supplemented with 25 mM Glc or Gal, treatment with Ins (100 nM), and treatment with Oligo (10 µg/ml) and BAM15 (10 µM) as indicated. Fluorescence was normalised to the Glc/control condition (details in the Experimental Procedures). Data presented as mean ± SEM, from 5 separate experiments. MMP, mitochondrial membrane potential. ***D-F***, Mature primary adipocytes were isolated from rats and incubated in assay media supplemented with 5 mM glucose (Glc) or galactose (Gal). In ***D***, adipocytes were treated without (control, Ctrl) or with Ins (20 nM) for 1 h. Following treatment, lactate content was determined enzymatically following MeOH-$CHCl_3$ extraction and normalised to the Glc/Ins condition. Data presented as mean + SEM, from 3 separate experiments. In ***E***, respiration was measured using the Oroboros O2K following the addition of Ins (20 nM), Oligo (5 µg/ml), carbonyl cyanide-4-(trifluoromethoxy)phenylhydrazone (FCCP, concentrations as indicated), Rot (10 µM), and AA (25 µM). Respiration was normalised to the baseline respiration of the Glc/Ins condition. Data presented as mean + half-range, from 2 separate experiments. In ***F***, respiration was measured as in (***E***). Data presented as mean + SEM, from 4 separate experiments. ***G***, Schematic depicting how the contribution of glucose to respiration-derived CO_2 was determined using ECAR (extracellular acidification rate), lactate production, and glucose oxidation data. Details in the main text. Data presented as mean ± SEM, derived from experiments cited in the main text. AUC, area under the curve; PPR, proton production rate.

Figure 2. Glucose is required for insulin to increase mitochondrial oxidant levels. ***A-B***, 3T3-L1 adipocytes were incubated in Media CX supplemented with 25 mM glucose (Glc) or galactose (Gal), and extracellular acidification rate (ECAR, ***A***) or cellular respiration (JO_2, ***B***) was measured using the XFp Analyzer following sequential treatment with insulin (Ins, 100 nM), dichloroacetate (DCA, 1 mM), oligomycin (Oligo, 10 µg/ml), and BAM15 (10 µM). Data presented as mean ± SEM, from 4 separate experiments. ***C***, 3T3-L1 adipocytes were serum-starved in Media BS with 25 mM Glc. During the last 1 h of serum-starvation, cells were pre-treated with DCA (1 mM) or antimycin A (AA, 50 nM). Cells were then incubated in Media BS, supplemented with 25 mM Glc or Gal, with Ins (100 nM) and DCA (1 mM) for the indicated times. Following treatment, cells were harvested and lysates were subjected to Western blotting with antibodies against the indicated proteins. Data representative of 4 separate experiments. D, dimer; M, monomer. ***D***, Densitometry of PRDX2 and PRDX3 bands from (***C***), expressed as a ratio of dimer to monomer bands, and made relative to the treatment with Glc at t=0 min. Data presented as mean ± SEM, from 4 separate experiments. ***E***, Densitometry of the indicated proteins from (***C***), normalised to α-tubulin and made relative to the Glc/t=20 min condition. Data presented as mean ± SEM, from 4 separate experiments. ***F***, 3T3-L1 adipocytes were serum-starved, then incubated in Media BS with Ins (100 nM), AA (50 nM), and/or cytochalasin B (CB, 25 µM). This treatment media was also supplemented with the indicated concentration of Glc, with the final volume balanced with either water or Gal (for the latter, the final combined sugar concentration was 25 mM). Following 1 h of treatment, cells were harvested and lysates subjected to Western blotting with antibodies against the indicated proteins. Data representative of 4 separate experiments. ***G***, Densitometry of PRDX3 bands from (***F***), expressed as the ratio of dimer to monomer bands, and made relative to the treatment with 25 mM Glc without Ins (second lane in ***F***). Data presented as mean ± SEM, from 4 separate experiments. ***H***, PRDX3 dimerisation (***G***) plotted against Glc uptake (Fig S2C) for Ins-treated cells exposed to varying media Glc concentrations. Hill equation fitted based on individual datapoints and overlayed onto data, which is presented as mean ± SEM, from 4 separate experiments.

Figure 3. Glucose-dependent mitochondrial oxidants do not cause insulin resistance. ***A***, Schematic depicting how insulin-dependent glucose oxidation could lead to oxidant-induced insulin resistance. 1) glucose is taken up and 2) a majority is diverted to fates such as lipid or lactate production (Quek *et al*., *manuscript under review*; (21)). 3) A small portion of glucose is oxidised and while this does not contribute substantially to respiration, 4) it increases mitochondrial reactive oxygen species (ROS) levels, 5) eventually leading to insulin resistance. GLUT4, glucose transporter 4. ***B-D***, 3T3-L1 adipocytes were treated in Media B with mitoparaquat (mPQ, 20 μM), dichloroacetate (DCA, 1 mM), and insulin (Ins, 100 nM) at the times indicated in (***B***). Cells were also treated with auranofin (AF, 5 μM) at t = 30 min (concurrently with mPQ treatment) in (***C***). Cells in (***C***) and (***D***) were treated in parallel. Following treatment, cells were either (***C***) harvested for protein and lysates were subjected to Western blotting with antibodies against the indicated proteins, or (***D***) assayed for 2-deoxyglucose uptake under cold conditions. In (***C***), densitometric analysis was performed as described in Fig 2D. Data presented as mean + SEM, from 4 separate experiments. *, $p<0.05$ and ns, $p>0.05$, by two-sample *t*-test. ***E***, 3T3-L1 adipocytes constitutively expressing HA-tagged GLUT4 were incubated in Media B and stimulated with insulin (Ins, 100 nM) for the indicated time-points, after which GLUT4 translocation to the plasma membrane (PM) was measured. Data presented as mean ± SEM, from 3 separate experiments.

Figure 4. Mitochondrial oxidants need to increase prior to the insulin stimulus to cause insulin resistance. ***A-B***, 3T3-L1 adipocytes constitutively expressing HA-tagged glucose transporter 4 (GLUT4) were incubated in Media B and treated with mitoparaquat (mPQ, 20 μM) and insulin (Ins, 100 nM) at the indicated time-points (*left panel*). Once a drug was added, it remained in the media for the remainder of the treatment period. Following treatment, cells were assayed for GLUT4 translocation to the plasma membrane (PM) (*middle panel*), or harvested and lysates were subjected to Western blotting with antibodies against the indicated proteins (*right panel*). Densitometric analysis (*right panel*) was performed as described in Fig 2D. Data in middle panel presented as mean + SEM, from 3 separate experiments. Data in right panel representative of 2 separate experiments. D, dimer; M, monomer. *, $p<0.05$ and ns, $p>0.05$, compared to Ins-treated cells, by two-sample *t*-test. ***C***, Schematic depicting how glucose metabolism demonstrates a disconnect between insulin-stimulated mitochondrial respiration and oxidant production in adipocytes. Details in the main text. ROS, reactive oxygen species.

FIGURE 1

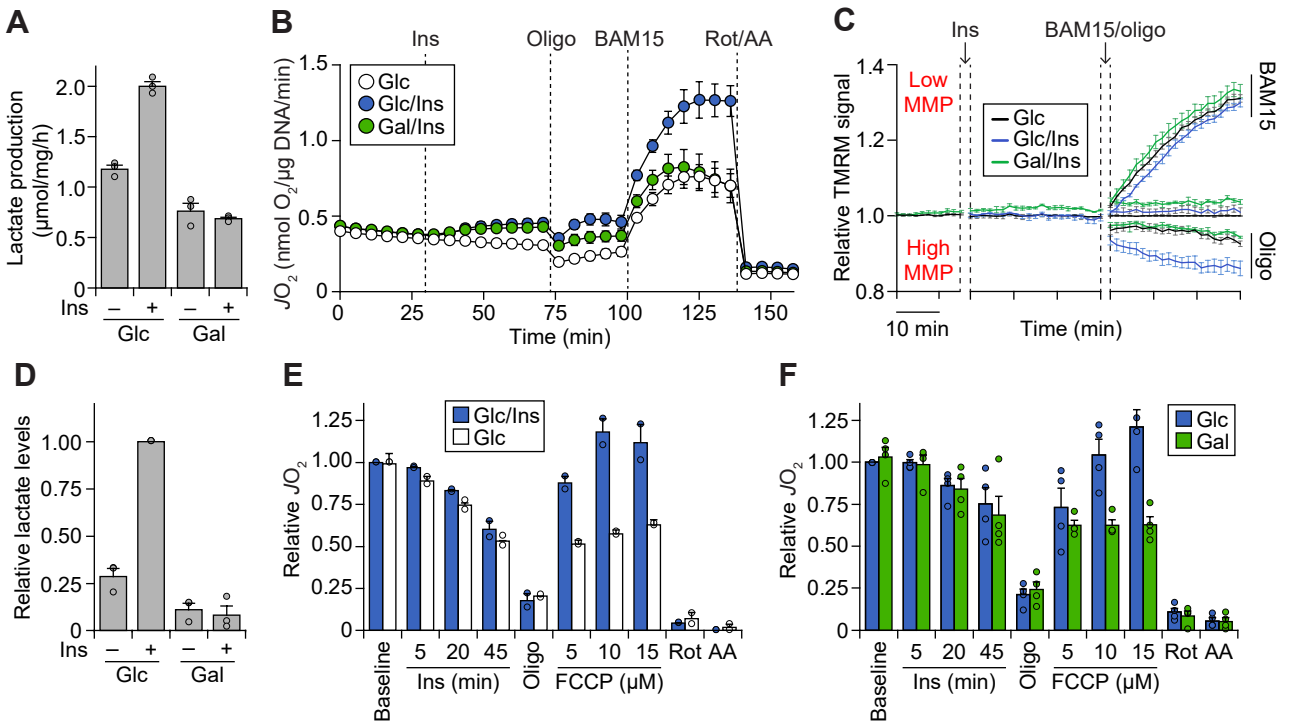

G

AUC ECAR (888.0 ± 83.1 mpH/h)
← Buffering capacity (11.8 µM/mpH)
← Measurement volume = 2.28 µl
← K_{vol} adjustment factor = 1.19

Total PPR (28.4 ± 2.7 nmol H^+/h)
← Lactate production (13.1 ± 0.4 nmol/h)

PPR due to CO_2 (15.3 ± 2.7 nmol H^+/h)
← Solubility of CO_2 in water (~95.3%)

CO_2 production (16.0 ± 2.8 nmol/h)
← CO_2 from glucose (3.2 ± 0.1 nmol/h)

Contribution of glucose to respiration-derived CO_2 (19.8%)

FIGURE 2

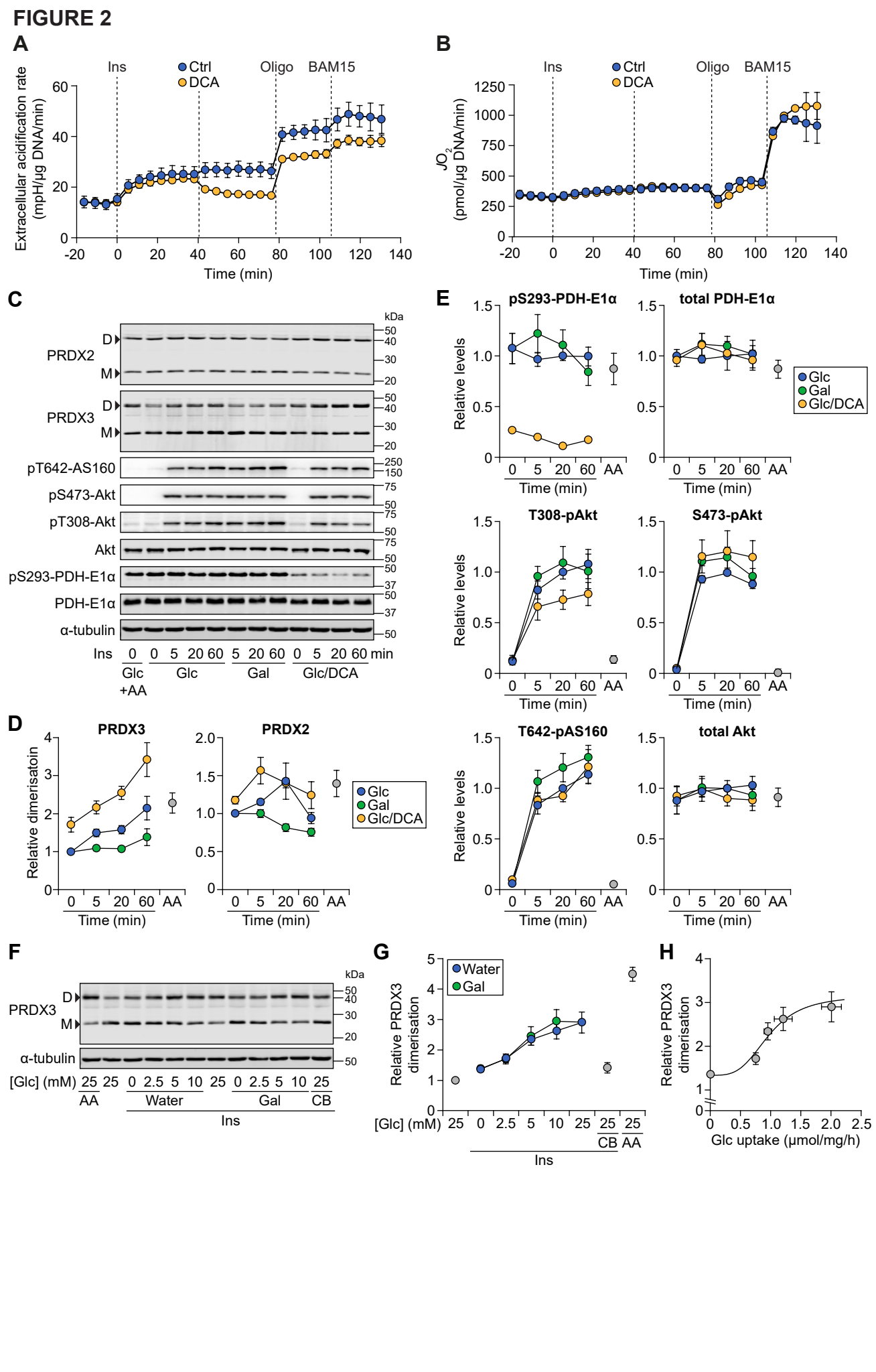
A
Ins
Ctrl
DCA
Oligo
BAM15
Extracellular acidification rate (mpH/µg DNA/min)
Time (min)
B
Ins
Ctrl
DCA
Oligo
BAM15
JO2 (pmol/µg DNA/min)
Time (min)
C
kDa
PRDX2
D
M
PRDX3
D
M
pT642-AS160
pS473-Akt
pT308-Akt
Akt
pS293-PDH-E1α
PDH-E1α
α-tubulin
Ins 0 0 5 20 60 5 20 60 0 5 20 60 min
Glc +AA
Glc
Gal
Glc/DCA
D
PRDX3
PRDX2
Relative dimerisatoin
Time (min)
Glc
Gal
Glc/DCA
E
pS293-PDH-E1α
total PDH-E1α
T308-pAkt
S473-pAkt
T642-pAS160
total Akt
Relative levels
Time (min)
Glc
Gal
Glc/DCA
F
kDa
PRDX3
D
M
α-tubulin
[Glc] (mM) 25 25 0 2.5 5 10 25 0 2.5 5 10 25
AA
Water
Gal
CB
Ins
G
Water
Gal
Relative PRDX3 dimerisation
[Glc] (mM) 25 0 2.5 5 10 25 25 25
CB
AA
Ins
H
Relative PRDX3 dimerisation
Glc uptake (µmol/mg/h)

FIGURE 3

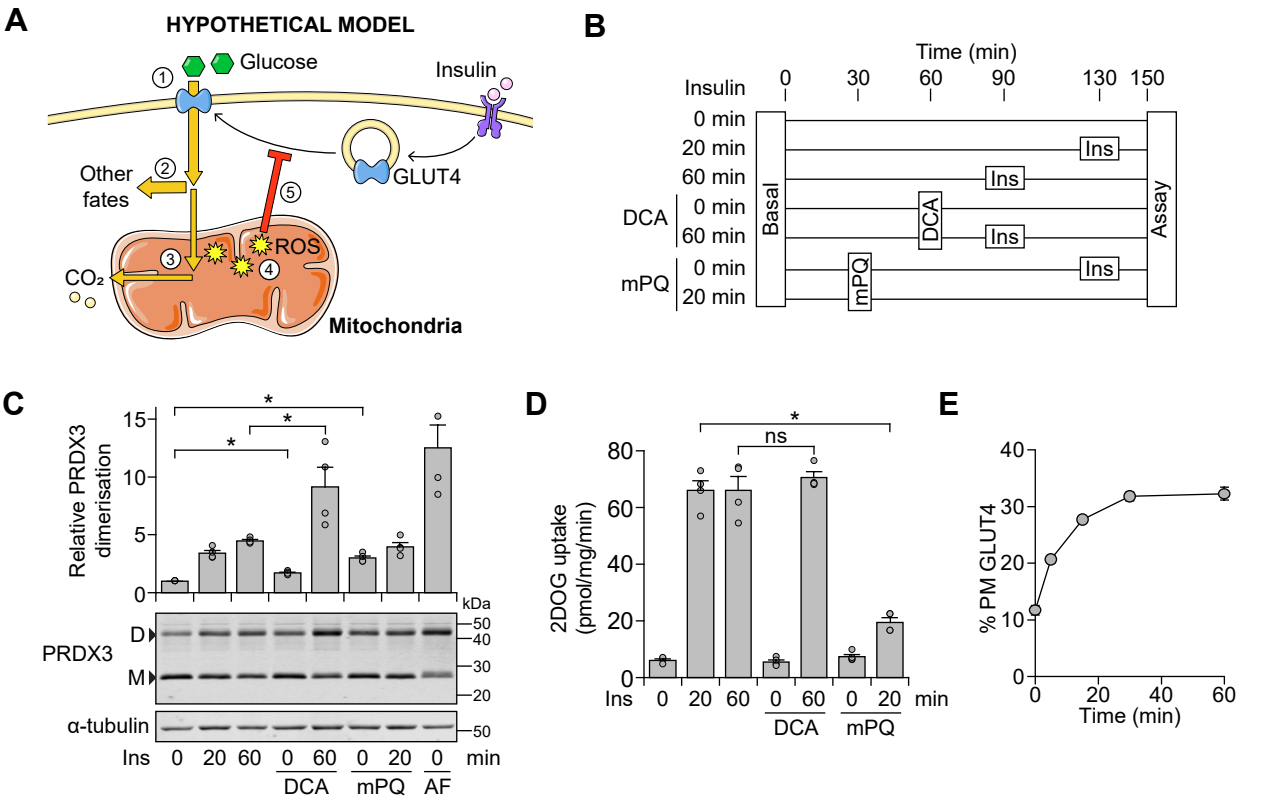
A
HYPOTHETICAL MODEL
Glucose
Insulin
GLUT4
Other fates
ROS
CO₂
Mitochondria
B
Time (min)
Insulin
0 30 60 90 130 150
0 min
20 min
60 min
DCA
0 min
60 min
mPQ
0 min
20 min
Basal
DCA
mPQ
Ins
Assay
C
Relative PRDX3 dimerisation
kDa
PRDX3
D
M
α-tubulin
Ins 0 20 60 0 60 0 20 0 min
DCA
mPQ
AF
D
2DOG uptake (pmol/mg/min)
ns
Ins 0 20 60 0 60 0 20 min
DCA
mPQ
E
% PM GLUT4
Time (min)

FIGURE 4

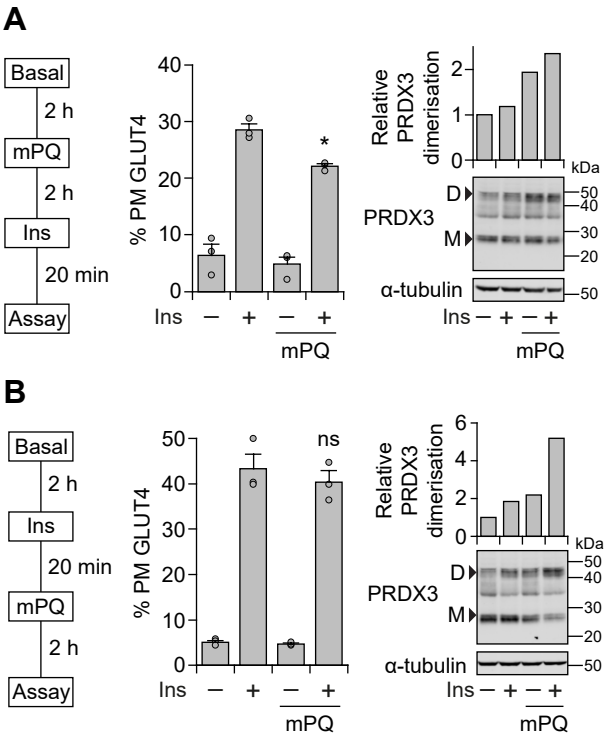
A
Basal
2 h
mPQ
2 h
Ins
20 min
Assay
% PM GLUT4
Ins
mPQ
Relative PRDX3 dimerisation
kDa
PRDX3
D
M
α-tubulin
B
ns
C
Glucose
Insulin
GLUT4
Amino acids
ROS
CO₂
?
PREVIOUSLY

Mitochondrial oxidants, but not respiration, are sensitive to glucose in adipocytes

James R. Krycer, Sarah D. Elkington, Alexis Diaz-Vegas, Kristen C. Cooke, James G. Burchfield, Kelsey H. Fisher-Wellman, Gregory J. Cooney, Daniel J. Fazakerley and David E. James

J. Biol. Chem. published online November 19, 2019
